Level Set Based Segmentation with Intensity and Curvature Priors

Michael E. Leventon[1]   Olivier Faugeras[1,2]   W. Eric L. Grimson[1]   William M. Wells III[1,3]

[1] MIT AI Lab
Cambridge, MA 02139
leventon, welg, sw@ai.mit.edu

[2] INRIA
Sophia Antipolis, France
Olivier.Faugeras@sophia.inria.fr

[3] Surgical Planning Lab
Brigham and Women's Hospital
Boston, MA 02115

Abstract

A method is presented for segmentation of anatomical structures that incorporates prior information about the intensity and curvature profile of the structure from a training set of images and boundaries. Specifically, we model the intensity distribution as a function of signed distance from the object boundary, instead of modeling only the intensity of the object as a whole. A curvature profile acts as a boundary regularization term specific to the shape being extracted, as opposed to simply penalizing high curvature. Using the prior model, the segmentation process estimates a maximum a posteriori higher dimensional surface whose zero level set converges on the boundary of the object to be segmented. Segmentation results are demonstrated on synthetic data and magnetic resonance imagery.

1 Introduction

Medical image processing applications such as surgical planning, navigation, simulation, diagnosis, and therapy evaluation all benefit from segmentation of anatomical structures from medical images. By segmentation, we refer to the process of labeling individual voxels in the volumetric scan by tissue type, based on properties of the observed intensities as well as anatomical knowledge about normal subjects.

Segmentation is typically performed using a mix of automated techniques and semi-automated techniques. With CT data, segmentation of some structures can be performed just using intensity thresholding. In general, however, segmentation is challenging and requires more sophisticated algorithms and significant human input. For example, the distribution of intensity values corresponding to one structure may vary throughout the structure and also overlap those of another structure, defeating intensity-based segmentation techniques. The strength of an "edge" at the boundary of the structure may vary or be weak relative to the texture inside the object, creating difficulties for gradient-based boundary detection methods.

Boundary finding segmentation methods such as Snakes [8], are generally local algorithms that require some feature (such as an edge) to be present along the boundary of the object, and gravitate toward that feature. These methods may be sensitive to the starting position and may "leak" through the boundary of the object if the edge feature is not salient enough in a certain region in the image.

Level set segmentation involves solving the energy-based active contours minimization problem by the computation of geodesics or minimal distance curves [2, 9, 12]. In this approach, a curve is embedded as a zero level set of a higher dimensional surface (Figure 1) [13, 16]. The entire surface is evolved to minimize a metric defined by the curvature and image gradient.

In [20], segmentation is performed by evolving a curve to maximally separate predetermined statistics inside and outside the curve. Paragios and Deriche in [14], build prior texture models and perform segmentation by combining boundary and region information. These methods include both global and local information, adding robustness to noise and weak boundaries and are formulated using level set techniques providing the advantages of numerical stability and topological flexibility.

Two common segmentation techniques, pixel classification based methods [5, 7] and boundary localization techniques [2, 8, 12, 20], typically include both an image term and a regularization term. In [6, 7], a regularization effect is included as a Markov prior expressing that structure labels should not vary sporadically in a local area (eliminating fragmentation). In [2, 8, 20], a smoothness term is added to penalize high curvature in the evolving curve. In [11], the regularizer penalizes only the smaller of the two curvatures when segmenting curve-like structures such as blood vessels. In most curve evolution methods, the amount of regularization required is a manually tuned parameter dependent on the shape properties of the object and noise in the image.

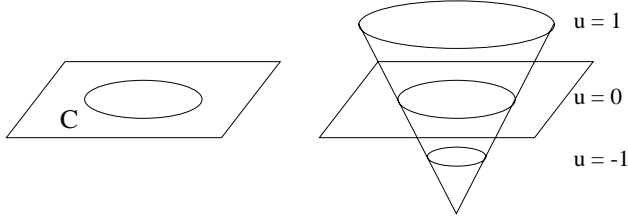Our method of segmentation incorporates prior informa-

Figure 1. Level sets of an embedding function u for a closed curve $\mathcal{C}$ in $\Re^2$.
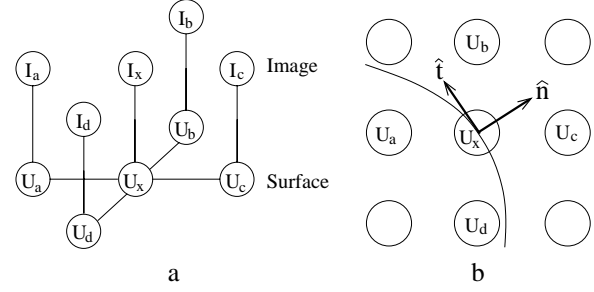

Figure 2. (a) Statistical dependency of node samples of the surface U and pixels of image I. (b) The directions of the normal and tangent of U are shown at the position x. The contour curve of height U_x is drawn.

tion about the intensity and curvature of the structure based on previously segmented training data. We model the distribution of intensity over the entire image as a function of the signed distance from the boundary of the structure. This provides a means of representing both changes of the intensity of the structure relative to its boundary and the intensity profiles of neighboring structures as a function of their distances to the object of interest. A distribution of the curvature of the structure is also modeled from the training data to determine the degree of regularization of the underlying level sets.

To segment an object from a novel image, we use the ideas of the level set techniques where the boundary curve is embedded as the zero level set of a higher dimensional surface. Unlike traditional level set techniques that maintain equivalence to minimizing an energy function over a curve, our method uses information over the entire image and higher dimensional surface. At every iteration, each position on the surface (representing a distance to the boundary) is adjusted towards a maximum *a posteriori* distance, based on the image information at that position and the values of neighboring points on the surface. The intensity-distance model directs the height of the surface towards a likely distance, and the curvature model keeps the surface regular.

2 The Prior Image-Surface Model

Given an image $I(\mathbf{x})$, the segmentation problem involves finding the closed curve $\mathcal{C}$ that lies along the boundary of the object of interest in the image. We define a surface U as the signed distance function to the curve $\mathcal{C}$. Therefore, $U(\mathbf{x})$ is both the height of the surface U at the position $\mathbf{x}$ and the signed distance from $\mathbf{x}$ to the nearest point on the curve $\mathcal{C}$. Instead of estimating the position of $\mathcal{C}$ directly, we estimate the value of U at every position $\mathbf{x}$ in the image. Once U is computed, the boundary of the object is found by extracting the zero level set of U.

We define a statistical dependency network over the surface U and the image I. To estimate the value $U_{\mathbf{x}}$ of U at a certain position $\mathbf{x}$ in the image, we maximize

$P(U_{\mathbf{x}} \mid I, U\backslash U_{\mathbf{x}})$, namely the probability of the height of the surface at that point, given the entire image and the rest of the surface. This expression is difficult to model, given all the dependencies. We therefore simplify the problem to a Markov network with only local dependencies. The links of the nodes in Figure 2a represent the dependencies considered. We assume the height of the surface at a certain point depends only on the intensity value of the image at that point, and the neighboring heights of the surface. This assumption can be expressed as:

$$P\left(U_{\mathbf{x}} \mid I,\, U\backslash U_{\mathbf{x}}\right) = P\left(U_{\mathbf{x}} \mid I_{\mathbf{x}},\, U_{\mathcal{N}(\mathbf{x})}\right) \qquad (1)$$

where $\mathcal{N}(\mathbf{x})$ is the neighborhood of $\mathbf{x}$.

Using properties of our network, we derive an expression for the above probability consisting of terms we will estimate from a set of training data.

$$P(U_{\mathbf{x}} \mid I_{\mathbf{x}}, U_{\mathcal{N}(\mathbf{x})}) = \frac{P(U_{\mathbf{x}}, I_{\mathbf{x}}, U_{\mathcal{N}(\mathbf{x})})}{P(I_{\mathbf{x}}, U_{\mathcal{N}(\mathbf{x})})} \qquad (2)$$

$$= \frac{P(I_{\mathbf{x}}, U_{\mathbf{x}})}{P(I_{\mathbf{x}}, U_{\mathcal{N}(\mathbf{x})})} \frac{P(U_{\mathbf{x}}, I_{\mathbf{x}}, U_{\mathcal{N}(\mathbf{x})})}{P(I_{\mathbf{x}}, U_{\mathbf{x}})} \qquad (3)$$

$$= \frac{P(I_{\mathbf{x}}, U_{\mathbf{x}})}{P(I_{\mathbf{x}}, U_{\mathcal{N}(\mathbf{x})})} P(U_{\mathcal{N}(\mathbf{x})} \mid I_{\mathbf{x}}, U_{\mathbf{x}}) \qquad (4)$$

$$= \frac{P(I_{\mathbf{x}}, U_{\mathbf{x}}) P(U_{\mathcal{N}(\mathbf{x})} \mid U_{\mathbf{x}})}{P(I_{\mathbf{x}}, U_{\mathcal{N}(\mathbf{x})})} \qquad (5)$$

The definition of conditional probability is used in Equations 2 and 4, and we are multiplying by the identity in Equation 3. In the final expression, we note that when conditioned on $U_{\mathbf{x}}$, the heights of the surface at neighboring locations do not depend on $I_{\mathbf{x}}$.

The first term in Equation 5 is the *image term*, that relates the intensity and the surface at $\mathbf{x}$. The next term relates the neighborhood of U about $\mathbf{x}$ to $U_{\mathbf{x}}$, and will act as a *regularization term*. The following two sections describe a
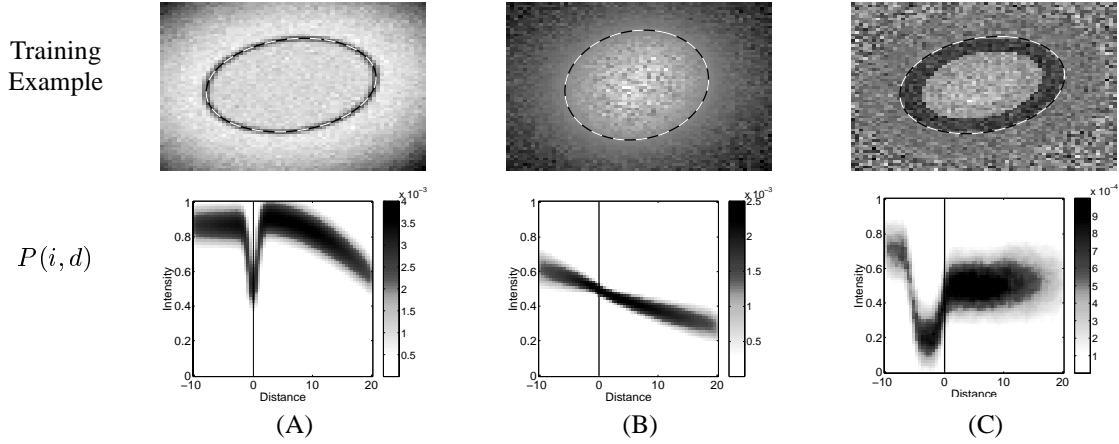
Figure 3. Top: One example of three training sets of random ellipses under different imaging conditions The dotted contour shows the boundary of the object. Bottom: The joint intensity/distance-to-boundary PDF derived from the training set. Left and right of the black vertical line indicate the intensity profile inside and outside the object.

means of estimating these functions based on prior training data. The denominator of Equation 5 does not depend on $U_{\mathbf{x}}$, and thus is ignored during the estimation process.

2.1 Intensity Model

We define a joint distribution model, $P(i, d)$, that relates intensity values, i, to signed distances d, based on a set of training images and training segmentations. Let $\{I_1, I_2, \ldots, I_n\}$ be a set of images of the same modality containing the same anatomical structure of various subjects and $\{\mathcal{C}_1, \mathcal{C}_2, \ldots, \mathcal{C}_n\}$ be the set of corresponding segmented boundary curves of the anatomical structure. Let U_j be the signed distance map to the closed curve $\mathcal{C}_j$. The training set $\mathcal{T}$, is a set of image-surface pairs, $\mathcal{T} = \{\langle I_1, U_1 \rangle, \ldots, \langle I_n, U_n \rangle\}$. We use a Parzen window density estimator with a Gaussian windowing function to model the joint distribution. The PDF is the mean of many 2D Gaussians centered at the positions $\langle I_j(\mathbf{x}), U_j(\mathbf{x}) \rangle$ for every pixel in every training image:

$$P(i,d) = \frac{1}{Z} \sum_{j=1}^{n} \sum_{\mathbf{x} \in \mathcal{X}} e^{\left(-\frac{(i - I_j(\mathbf{x}))^2}{2\sigma_i^2} - \frac{(d - U_j(\mathbf{x}))^2}{2\sigma_d^2} \right)} \tag{6}$$

where $\mathcal{X}$ is the set of all positions in the image, σ_i and σ_d are the variances of the Parzen kernel, and the normalization factor $Z = (2\pi\sigma_i\sigma_d n|\mathcal{X}|)^{-1}$.

Figure 3 illustrates the estimated joint probability density functions for random ellipses with various contrast scenarios. Notice that Ellipse A can be easily segmented using a gradient based method, but cannot be thresholded, as the intensity distribution inside and outside the object overlap significantly. On the other hand, simple gradient

methods would fail to extract Ellipse B due to high texture, while a single intensity threshold isolates the object. Neither scheme would work for Ellipse C, as higher level knowledge is required to know which edge is the correct boundary.

Figure 4 illustrates the estimated joint PDFs for the corpus callosum and slices of two acquisitions of the femur. In the sagittal scan of the femur (Figure 4d), the dark layer around the brighter, textured region is cortical bone, which gives essentially no MR signal. Without prior knowledge of the intensity distribution of the entire femur, the cortical bone could easily be missed in a segmentation. However, by training a joint distribution over intensity and signed distance, we generate a PDF that encodes the fact that the dark region is a part of the object. This example is similar to the synthetic ellipse in Figure 4a.

2.2 Curvature Model

Boundary detection methods commonly use a regularization term to uniformly penalize regions of high curvature, independent of the structure being segmented [8, 2, 20]. Our goal is to use the term $P(U_{\mathcal{N}(\mathbf{x})} \mid U_{\mathbf{x}})$ as a local regularizer, but one that can be estimated from a set of training data, and thereby tuned to the appropriate application. One method of modeling this function is to create a 5D Parzen joint PDF over $U_{\mathbf{x}}$ and its four neighbors. A drawback of this approach is that a 5D space is difficult to fill and thus requires many training samples. Furthermore, the neighborhood depends on the embedded coordinate system, and would give different results based on the pose of the object in the image (consider a square aligned with the axes versus one rotated by $45°$). Therefore, instead of considering
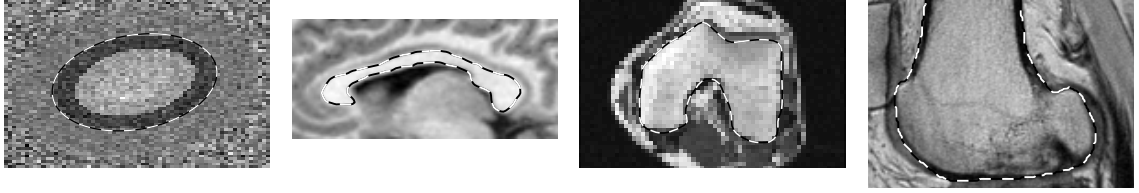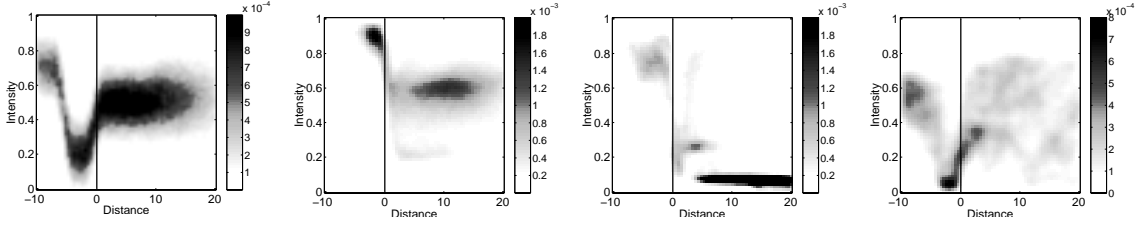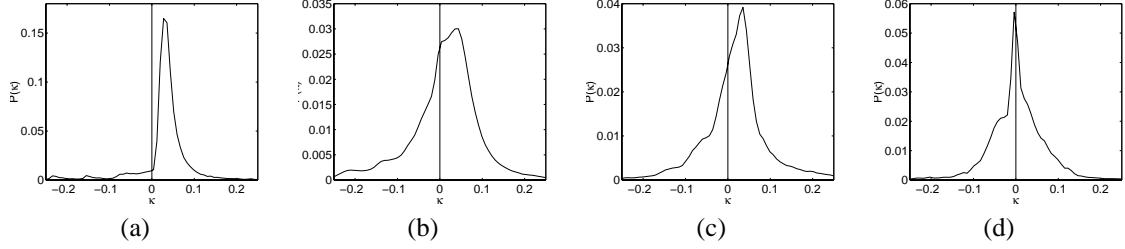
Figure 4. Top: One example of each of four training sets of objects. Middle: The joint intensity/distance-to-boundary PDF derived from the training set. Bottom: The curvature profile of each object class. Notice that the ellipse class has only positive curvature.

the four neighbors (two horizontal and two vertical) in the "arbitrary" embedded coordinate system, we use four (interpolated) neighbors in the direction of the local normal $(\hat{n})$ and tangent $(\hat{t})$ to the embedded curve (see Figure 2b). In other words, we reparameterize to an intrinsic coordinate system based on the surface:

$$
\begin{aligned}
P(U_{\mathcal{N}(\mathbf{x})} \mid U_{\mathbf{x}}) &= P(U_{h+}, U_{h-}, U_{v+}, U_{v-} | U_{\mathbf{x}}) \quad (7) \\
&= P(U_{\hat{n}+}, U_{\hat{n}-}, U_{\hat{t}+}, U_{\hat{t}-} | U_{\mathbf{x}}) \quad (8) \\
&= P(U_{\hat{n}+}, U_{\hat{n}-} | U_{\mathbf{x}}) P(U_{\hat{t}+}, U_{\hat{t}-} | U_{\mathbf{x}}) \quad (9)
\end{aligned}
$$

The last step makes the assumption that the neighbors in the normal direction and those in the tangent direction are conditionally independent given $U_{\mathbf{x}}$.

We now model the terms in Eq. 9 based on properties of the surface U and prior knowledge of the boundary to be segmented. While U is considered to be a finite network of nodes and $U_{\mathbf{x}}$ a particular node, we define $u(\mathbf{x})$ to be the analogous continuous surface over $\mathbf{x}$. We derive the relationship between $U_{\mathbf{x}}$ and its neighbors by considering the first and second derivatives of $u(\mathbf{x})$ in the directions of the normal and tangent to the level set at $\mathbf{x}$. The unit normal and unit tangent to the underlying level set of u are defined as:

$$
\hat{\mathbf{n}} = \frac{\nabla u}{|\nabla u|} = \frac{1}{(u_x^2 + u_y^2)^{\frac{1}{2}}} \begin{bmatrix} u_x \\ u_y \end{bmatrix} \quad (10)
$$

$$
\hat{\mathbf{t}} = \frac{1}{(u_x^2 + u_y^2)^{\frac{1}{2}}} \begin{bmatrix} -u_y \\ u_x \end{bmatrix} \quad (11)
$$

To compute the directional derivatives, we first evaluate the second-order Taylor expansion of u at $\mathbf{x}$ in the arbitrary direction of $\mathbf{w}$:

$$
u(\mathbf{x} + \lambda\mathbf{w}) = u(\mathbf{x}) + \lambda\frac{\partial u}{\partial \mathbf{x}}\mathbf{w} + \frac{\lambda^2}{2}\mathbf{w}^{\mathsf{T}}\frac{\partial^2 u}{\partial \mathbf{x}^2}\mathbf{w} + \dots \quad (12)
$$

which yields a general expression for derivatives of u in the direction of $\mathbf{w}$:

$$
\frac{\partial u}{\partial w} = \frac{\partial u}{\partial \mathbf{x}}\mathbf{w} \quad (13)
$$

$$
\frac{\partial^2 u}{\partial w^2} = \mathbf{w}^{\mathsf{T}}\frac{\partial^2 u}{\partial \mathbf{x}^2}\mathbf{w} \quad (14)
$$

Evaluating the first partial in both the directions of $\hat{\mathbf{n}}$ and $\hat{\mathbf{t}}$ yields:

$$
\frac{\partial u}{\partial \hat{n}} = \frac{\partial u}{\partial \mathbf{x}}\hat{\mathbf{n}} = |\nabla u| \quad (15)
$$

$$
\frac{\partial u}{\partial \hat{t}} = \frac{\partial u}{\partial \mathbf{x}}\hat{\mathbf{t}} = 0 \quad (16)
$$

These results are not surprising given that $\hat{\mathbf{n}}$ by definition lies in the direction of the gradient. Note that when u is a signed distance map, $\frac{\partial u}{\partial \hat{n}} = |\nabla u| = 1$.

We now compute expressions for the second derivatives:

$$\frac{\partial^2 u}{\partial \hat{n}^2} = \hat{\mathbf{n}}^\top \frac{\partial^2 u}{\partial \mathbf{x}^2} \hat{\mathbf{n}} = \frac{u_{xx}u_x^2 + 2u_{xy}u_xu_y + u_{yy}u_y^2}{u_x^2 + u_y^2} \quad (17)$$

$$\frac{\partial^2 u}{\partial \hat{t}^2} = \hat{\mathbf{t}}^\top \frac{\partial^2 u}{\partial \mathbf{x}^2} \hat{\mathbf{t}} = \frac{u_{xx}u_y^2 - 2u_{xy}u_xu_y + u_{yy}u_x^2}{u_x^2 + u_y^2} \quad (18)$$

In the special case when u is a signed distance function, it can be shown that $\frac{\partial^2 u}{\partial \hat{n}^2} = 0$ and $\frac{\partial^2 u}{\partial \hat{t}^2} = \kappa$ where the curvature of the underlying level set, κ, is given as:

$$\kappa = \frac{u_{xx}u_y^2 - 2u_xu_yu_{xy} + u_{yy}u_x^2}{(u_x^2 + u_y^2)^{\frac{3}{2}}} \quad (19)$$

In summary, here are the values of the first and second partial derivatives of u in the tangent and normal directions under the constraint that the surface u is a continuous signed distance map:

$$\frac{\partial u}{\partial \hat{n}} = 1 \qquad \frac{\partial u}{\partial t} = 0$$

$$\frac{\partial^2 u}{\partial \hat{n}^2} = 0 \qquad \frac{\partial^2 u}{\partial \hat{t}^2} = \kappa \quad (20)$$

We can use this information about the ideal distance map and underlying curvatures to regularize U at $\mathbf{x}$. Consider the formulas for (centered) finite differences of an arbitrary 1D function.

$$\frac{df(x)}{ds} \approx \frac{f(x+s) - f(x-s)}{2s} \quad (21)$$

$$\frac{d^2f(x)}{ds^2} \approx \frac{f(x+s) + f(x-s) - 2f(x)}{s^2} \quad (22)$$

Notice that $f(x)$ does not appear in $\frac{df(x)}{ds}$, indicating that changing f only at one position at a time cannot change the local slope. However, changing $f(x)$ does directly affect the second derivative, so we model the relationship between $U_\mathbf{x}$ and its neighbors to adhere to the second derivative constraints.

We define the likelihood of the neighbors in the normal direction to be:

$$P(U_{\hat{n}+}, U_{\hat{n}-} | U_\mathbf{x}) = \frac{1}{Z_1} \exp\left(-\frac{(U_{\hat{n}+} + U_{\hat{n}-} - 2U_\mathbf{x})^2}{2\sigma_1^2}\right) \quad (23)$$

where Z_1 is a normalization factor and σ_1 determines the strength of the constant-normal-direction constraint. This has the effect of keeping the gradient magnitude of the surface constant (however not necessarily 1), preventing the surface from evolving arbitrarily. Typically one needs to extract the zero level set and reinitialize the distance function from time to time during the evolution. This direction of regularization reduces the need to reinitialize the surface.

As for the likelihood of the neighbors in the tangent direction, we seek an expression that takes into account the curvature profile of the training data. A convex shape, for example, has non-negative curvature everywhere, so if the training set consists of all convex shapes, the level sets of the surface should stay convex throughout the estimation. The fact that a polygon has bi-modal curvature (0 and ∞) could be used to define a polygon-finder, if the surface can be constrained to match the distribution of curvatures of the training set. For each training surface, U_j, we compute a curvature map κ_j using Equation 19. We then define a PDF which encourages the curvature as reflected in the discrete differences $(U_{\hat{t}+} + U_{\hat{t}-} - 2U_\mathbf{x})$ to be consistent with curvatures observed in the training data $(\kappa_j(\mathbf{x}))$. The PDF is derived using Parzen windowing, similar to the intensity PDF defined in Section 2.1.

$$P(U_{\hat{t}+}, U_{\hat{t}-} | U_\mathbf{x}) = \quad (24)$$
$$\frac{1}{Z_2} \sum_{j=1}^{n} \sum_{\mathbf{x} \in \mathcal{X}} \exp\left(-\frac{\|(U_{\hat{t}+} + U_{\hat{t}-} - 2U_\mathbf{x}) - \kappa_j(\mathbf{x})\|^2}{2\sigma_2^2}\right)$$

The third row of Figure 4 shows the curvature profile of training sets of various objects.

In summary, the regularization of the surface is broken down into a regularization in the local normal and tangent directions. The second derivative in the normal direction is modeled as a zero mean, low variance Gaussian to keep the surface linear in that direction. A distribution over the second derivative in the tangent direction (e.g. the curvature of the level sets) is derived from the training data and used as an object-specific curvature regularization term.

3 Surface Estimation

In the previous section, we defined a model of the embedding surface of the boundary that we wish to estimate given a novel image. Starting with an initial closed curve, we build the higher dimensional surface by computing the signed distance to the curve at every point. Given the prior model and the image, the height of the surface at location $\mathbf{x}$ is related to the image intensity at $\mathbf{x}$ and the local neighborhood of the surface by the following equation:

$$P\left(U_\mathbf{x} \mid I_\mathbf{x}, U_{\mathcal{N}(\mathbf{x})}\right) \propto \quad (25)$$
$$\underbrace{P(I_\mathbf{x}, U_\mathbf{x})}_{\text{Image Term}} \underbrace{P(U_{\hat{t}+}, U_{\hat{t}-} | U_\mathbf{x})}_{\text{Curvature Term}} \underbrace{P(U_{\hat{n}+}, U_{\hat{n}-} | U_\mathbf{x})}_{\text{Linearity Term}}$$

We use this equation to re-estimate each surface point independently, maximizing its log probability while assuming the rest of the surface is constant.

$$U_\mathbf{x} = \max_{U_\mathbf{x}} \log P(U_\mathbf{x} \mid I_\mathbf{x}, U_{\mathcal{N}(\mathbf{x})}) \quad (26)$$

Instead of finding the global maximum of the PDF for each $U_\mathbf{x}$, we adjust $U_\mathbf{x}$ in the direction of increasing probability

towards the local maximum by differentiating the log probability in Equation 25.

$$U_{\mathbf{x}} = U_{\mathbf{x}} + \lambda \left(\frac{d}{dU_{\mathbf{x}}} \log P(U_{\mathbf{x}} \mid I_{\mathbf{x}}, U_{\mathcal{N}(\mathbf{x})}) \right) \qquad (27)$$

This update is repeated until there is little change in the surface. While small, local oscillations in the surface can occur if the step size λ is too high, in practice, an empirical value of λ can easily be found such that the surface evolves in reasonable time without oscillations.

The linearity regularization term that acts on the surface in the direction normal to the level set keeps the gradient magnitude locally constant, but in general the surface does not remain a true distance function. We therefore extract the boundary and reinitialize the distance map when the gradient magnitudes stray from 1. The regularization term greatly reduces the need to reinitialize, but it does not eliminate it. Typically reinitialization occurs once or twice during the segmentation, or about every 50 iterations.

For efficiency, most level set methods do not evolve the higher dimensional surface at every point over the image, but just in a narrow band around the boundary of the object [12]. As most level set segmentation methods are equivalent to curve energy minimization, the band size should not affect the results. Banding in this way can also be applied to our method of surface estimation, but clearly anything outside the band would not contribute to the surface estimation. In the 2D examples presented here, banding was not used, but for efficiency, banding will most likely be a necessity when the method is extended to 3D segmentation.

Some level set segmentation methods require a balloon force be added to the evolution when the initial curve is placed inside the object [2]. This is due to the fact that the regularization term by itself will shrink the evolving curve to a point if the boundaries are not close enough to the edge. A balloon force counteracts the regularization force and pushes the curve outward. In our method, a balloon force is generally not necessary even when starting only from inside the object, as the intensity vs. distance distribution will force the curve to grow or shrink as appropriate. However, in cases where the intensity distribution inside and outside the object are very similar (e.g. Figure 3A), only a force at the boundary is felt, which may not be strong enough to pull the zero level set to the edge. For cases such as this, a balloon force is added to the system to force the expansion.

4 Results

We report results of testing this method on synthetic data and 2D slices of MR data. Three sets of ellipses were used to test the algorithm under varying contrast conditions. In each case, a training set of 25 random ellipses was generated and used to derive the intensity and curvature model.

A novel random ellipse was generated using similar rendering for segmentation. Figure 5 shows the results of the segmentation. In the top row, there are two starting curves for the ellipse with the strong edge. In the first case only, (a), a small balloon force was required to push the curve outward, as described above. In case (b), the initial curve crossed the edge, so no balloon force was necessary. Figure 5c–d show the segmentations of the other two renderings. In (d), both the interior bright region and the dark boundary are included in the segmentation due to the prior intensity model, consistent with the training images.

The sensitivity to the initialization of the curve is dependent on the intensity profile of structure of interest relative to its background. In the synthetic image (a), the object and background have almost identical intensity distributions, making it locally indistinguishable whether the evolving curve lies inside or outside the object. Therefore, if part of the initial curve was initialized completely outside the object, then it would not disappear, causing an incorrect segmentation. Global shape information can be added to the segmentation process to correct the local ambiguity [10]. In the other segmentation examples, even though there is some amount of intensity overlap, the intensity profiles are different enough that the algorithm is robust to a wide range of initial conditions: the initial curve need not directly overlap or fall inside the structure of interest.

The segmentations of two corpora callosa are shown in Figure 6. The training set consisted of 48 segmented corpora callosa. Notice that the intensity distribution in Figure 4b is consistent and compact, despite the large number of images. Due to the topological invariance of the level set method, the contours grow, shrink, combine, and split to reach the final segmentation. The algorithm is generally robust to initialization, as long as some portion of the object lies inside the initial curve.

Figure 7 shows the segmentation of two slices of femurs from two different MR acquisitions. In each case, the training set consisted of the ten neighboring slices of the test slice. In the axial slices (a), the surface evolves such that the zero level set converges on the boundary of the femur. Notice that in the third image, the two dark spots in the femur create a "snag" for the zero level set as the distances for the dark intensities are much more likely to be outside the object. However, the neighborhood term distributes the information and pulls the region inside the object. Also note that there are other regions in the image with intensity values in the range of those inside the femur. One such region can be seen surrounded by the boundary in the lower left area of the third frame. Again, the neighboring information and curvature prior cause this region to correctly be left out of the segmentation.

The sagittal slice of the femur in (b) illustrates both a strength and a weakness of the method. The final bound-

ary successfully captures both the marrow inside the bone and the dark region of cortical bone at the boundary. Furthermore, the segmentation excludes the cartilage, which is the mid-tone semi-circular strip at the bottom of the image. However, the boundary does leak into the muscle located in the upper left as the intensities very closely match those of the interior of the femur. Using a texture measure in addition to the intensity could prevent this leakage.

5 Future Work

While the results presented here were on 2D imagery, the algorithm is easily extendable to 3D. In three dimensions, the boundary is a closed surface and the distance function is a 4D hyper-surface. The method of acquiring the prior intensity information would remain unchanged. The curvature prior would have to be adapted, as the level sets of the hyper-surface have two principal curvatures at every point. Instead of training on one curvature, the joint distribution of the first and second curvatures could be modeled, allowing shapes with a certain joint-curvature profile to be favored (as done explicitly with vessels in [11]). Also in the extension to 3D, some amount of banding may be necessary for efficiency, so that the hyper-surface is only updated in a band of a certain number of voxels away from the boundary.

Currently, our imaging model consists of relating intensity to distance from the boundary. However, other measures derived from the image can be used in this framework, such as image gradient (∇I), texture measurements, or even the image gradient in the intrinsic coordinate system of the level sets ($\nabla I \cdot \nabla U$). These other measures may be more appropriate for segmentation of some anatomical structures.

In conclusion, we have presented a novel method for segmenting anatomical structures that includes prior information about intensity and curvature as a function of distance to the object boundary. The approach uses the idea from existing level set methods of representing the boundary as the zero level set of a higher dimensional embedding function, and estimates the maximum *a posteriori* surface whose zero level set converges on the boundary of the object to be segmented.

References

[1] L. Ambrosio and H. M. Soner. Level set approach to mean curvature flow in arbitrary codimension. *J. of Diff. Geom.*, 43:693–737, 1996.

[2] V. Caselles, R. Kimmel, and G. Sapiro. Geodesic active contours. *Int'l J. Comp. Vision*, 22(1):61–79, 1997.

[3] L. D. Cohen. On active contour models and balloons. *CVGIP: Image Understanding*, 53(2):211–218, 1991.

[4] W. Freeman and E. Pasztor. Learning low-level vision. Technical report, Mitsubishi Electric Research Lab, 1999.

[5] G. Gerig *et al.* Unsupervised tissue type segmentation of 3d dual-echo MR head data. *Image and Vision Computing*, 10:349–360, 1992.

[6] K. Held *et al.* Markov random field segmentation of brain MR images. *IEEE Trans. Med. Imaging*, 16:878–887, 1998.

[7] T. Kapur. *Model Based Three Dimensional Medical Image Segmentation*. Ph.D. Thesis, Massachusetts Institute of Technology, Cambridge, MA, 1999.

[8] M. Kass, A. Witkin, and D. Terzopoulos. Snakes: Active contour models. *Int'l J. Comp. Vision*, 1(4):321–331, 1988.

[9] A. Kichenassamy, A. Kumar, P. Olver, A. Tannenbaum, and A. Yezzi. Gradient flows and geometric active contour models. In *IEEE Int'l Conf. Comp. Vision*, pages 810–815, 1995.

[10] M. Leventon, E. Grimson, and O. Faugeras. Statistical shape influence in geodesic active contours. In *Proc. IEEE Conf. Comp. Vision and Patt. Recog.*, 2000.

[11] L. M. Lorigo, O. Faugeras, W. Grimson, R. Keriven, R. Kikinis, and C.-F. Westin. Co-dimension 2 geodesic active contours for MRA segmentation. In *Int'l Conf. Inf. Proc. in Med. Imaging*, pages 126–139. Springer-Verlag, 1999.

[12] R. Malladi, J. Sethian, and B. Vemuri. Shape modeling with front propagation: A level set approach. *IEEE Trans. Patt. Analysis and Mach. Intell.*, 17(2):158–175, February 1995.

[13] S. Osher and J. Sethian. Fronts propagating with curvature-dependent speed: Algorithms based on Hamilton-Jacobi formulation. *J. of Comp. Physics*, 79(1):12–49, 1988.

[14] N. Paragios and R. Deriche. Geodesic active regions for supervided texture segmentation. In *IEEE Int'l Conf. Comp. Vision*, pages 926–932, 1999.

[15] G. Sapiro. Vector-valued active contours. In *Proc. IEEE Conf. Comp. Vision and Patt. Recog.*, pages 680–685, 1996.

[16] J. A. Sethian. *Level Set Methods*. Cambridge University Press, 1996.

[17] K. Siddiqi, Y. B. Lauzière, and A. Tannenbaum. Area and length minimizing flows for shape segmentation. *IEEE Trans. Image Processing*, 7(3):433–443, March 1998.

[18] L. Staib and J. Duncan. Boundary finding with parametrically deformable contour models. *IEEE Trans. Patt. Analysis and Mach. Intell.*, 14(11), 1992.

[19] H. Tek and B. Kimia. Image segmentation by reaction-diffusion bubbles. In *IEEE Int'l Conf. Comp. Vision*, pages 156–162, 1995.

[20] A. Yezzi, A. Tsai, and A. Willsky. A statistical approach to snakes for bimodal and trimodal imagery. In *IEEE Int'l Conf. Comp. Vision*, pages 898–903, 1999.
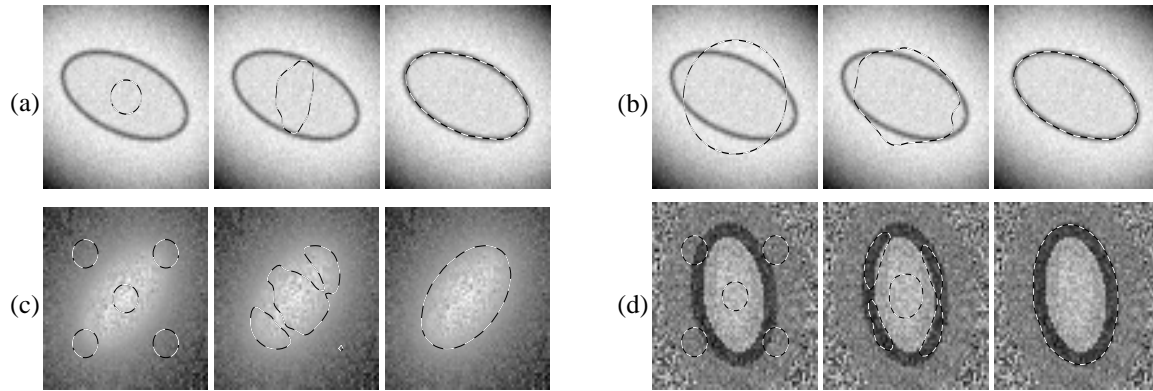
Figure 5. The results of segmenting various ellipses. Each group consists of the initial, middle, and final steps in the evolution with the zero level set of the surface overlaid. In each case, the training set consisted of random ellipses with similar rendering. A balloon force was added only for (a) as described in the text.
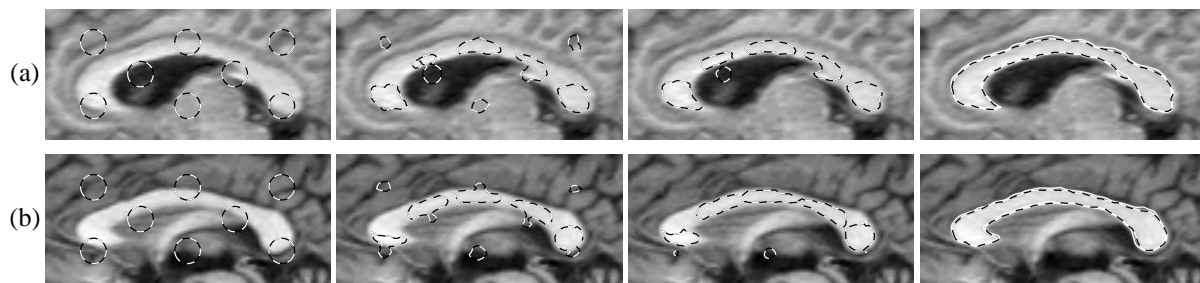

Figure 6. Initial, middle, and final steps in the segmentation two corpora callosa. The training set consisted of 48 other corpora callosa with the same MR imaging parameters.
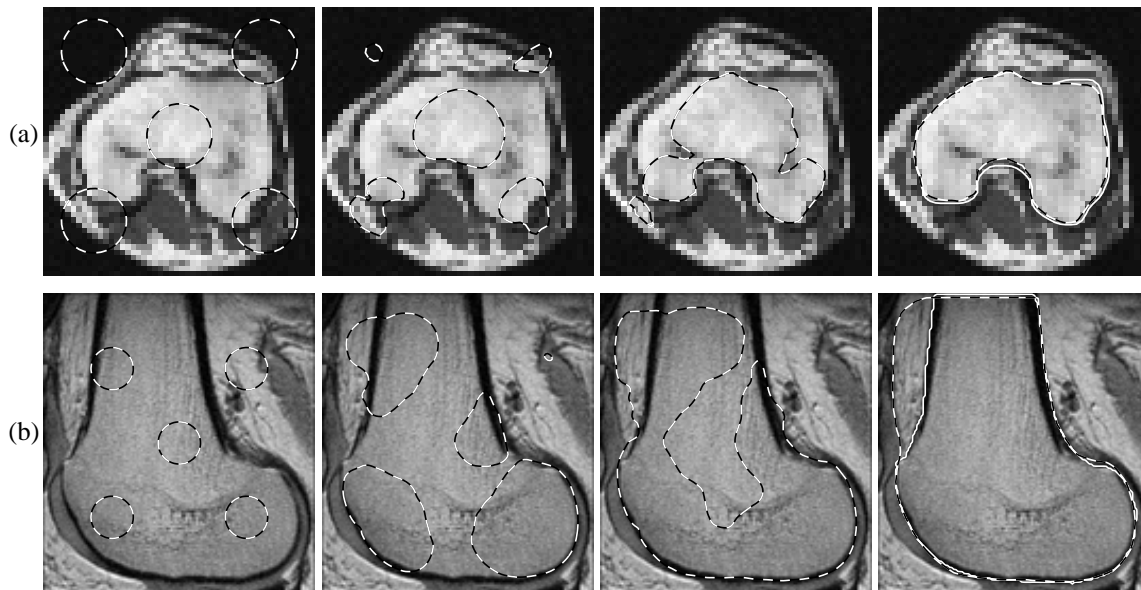

Figure 7. Initial, middle, and final steps in the 2D segmentation two acquisitions of the femur. In each case, the training set consisted of the ten neighboring slices of the test slice. The white curve in the last frame of each is the manually-segmented ground truth.